Modulation of magnetic behavior via ligand-field effects in the trigonal clusters (PhL)Fe3L*3 (L* = thf, py, PMe2Ph)

Chemical Science

Dynamic Article Links

Cite this: *Chem. Sci.*, 2012, **3**, 407

www.rsc.org/chemicalscience

EDGE ARTICLE

Modulation of magnetic behavior *via* ligand-field effects in the trigonal clusters (^{Ph}L)Fe$_3$L$^*_3$ (L* = thf, py, PMe$_2$Ph)†

Emily V. Eames, T. David Harris and Theodore A. Betley*

Received 21st July 2011, Accepted 3rd October 2011
DOI: 10.1039/c1sc00492a

Utilizing a hexadentate ligand platform, a series of trinuclear iron clusters (^{Ph}L)Fe$_3$L$^*_3$ (^{Ph}LH$_6$ = MeC(CH$_2$NPh-*o*-NPh)$_3$; L* = tetrahydrofuran (**1**), pyridine (**2**), PMePh$_2$ (**3**)) has been prepared. The phenyl substituents on the ligand sterically prohibit strong iron–iron bonding from occurring but maintain a sufficiently close proximity between iron centers to permit direct interactions. Coordination of the weak-field tetrahydrofuran ligand to the iron centers results in a well-isolated, high-spin $S = 6$ or $S = 5$ ground state, as ascertained through variable-temperature dc magnetic susceptibility and low-temperature magnetization measurements. Replacing the tetrahydrofuran ligands with stronger σ-donating pyridine or tertiary phosphine ligands reduces the ground state to $S = 2$ and gives rise to temperature-dependent magnetic susceptibility. In these cases, the magnetic susceptibility cannot be explained as arising simply from superexchange interactions between metal centers through the bridging amide ligands. Rather, the experimental data are best modelled by considering a thermally-induced variation in molecular spin state between $S = 2$ and $S = 4$. Fits to these data provide thermodynamic parameters of $\Delta H = 406$ cm^{-1} and $T_c = 187$ K for **2** and $\Delta H = 604$ cm^{-1} and $T_c = 375$ K for **3**. The difference in these parameters is consistent with ligand field strength differences between pyridine and phosphine ligands. To rationalize the spin state variation across the series of clusters, we first propose a qualitative model of the Fe$_3$ core electronic structure that considers direct Fe–Fe interactions, arising from direct orbital overlap. We then present a scenario, consistent with the observed magnetic behaviour, in which the σ orbitals of the electronic structure are perturbed by substitution of the ancillary ligands.

Introduction

Strong electronic and/or magnetic interactions between metal centers in polynuclear architectures can find significant utility in the design of various classes of magnetic materials, such as low-density permanent magnets,[1] single-molecule[2] and single-chain magnets,[3] and molecular wires.[4] The magnitude of these interactions is largely dictated by factors such as metal–metal separation and the type, if any, of bridging ligand. For instance, structurally symmetric bridging ligands, in conjunction with mixed-valence metal frameworks, can give rise to spin-dependent electron delocalization *via* a double exchange mechanism[5] and, consequently, well-isolated, high-spin ground states.[6] Additionally, superexchange between metal centers through diamagnetic bridging ligands, or direct exchange between a metal center and paramagnetic ligand, leads to ferromagnetic or antiferromagnetic coupling of electrons.

Alternatively, direct metal–metal interactions can arise when open-shell metal centers are not sterically prevented from engaging in direct M–M orbital overlap. The resulting interactions can range from single bond (*e.g.* Rh$_2$(OAc)$_4$)[7] to multiple bond configurations (*e.g.* Re$_2$Cl$_8$,[8] (Ar*)$_2$Cr$_2$).[9] The vast majority of coordination complexes that feature metal–metal bonding are composed of 4d and 5d transition metal ions or 3d ions in strong ligand fields (*e.g.*, CO) and in low oxidation states, giving rise to nearly exclusively low-spin ground states.[10,11] The resulting low-spin configurations preclude observation of the desired properties associated with the presence of unpaired electrons. Substituting weak field for strong field ligand sets with first-row transition ions typically leads to weak exchange interactions between metal ions, rather than metal–metal bonding, owing to their more contracted 3d-orbitals that preclude sufficient M–M orbital overlap. Nevertheless, the possibility does exist to enforce direct M–M orbital overlap, creating weak bonding interactions without maximal pairing of the metal valence electrons.

Within polynuclear clusters, it is often difficult to predictably dictate the coordination environments or electronic structure of the individual metal ions or the molecule as a whole.[12] One potential method for achieving these design criteria is employment of a polydentate ligand structure within which the

Department of Chemistry and Chemical Biology, Harvard University, Cambridge, MA, 02139, USA. E-mail: betley@chemistry.harvard.edu

† Electronic supplementary information (ESI) available. CCDC reference numbers 789355–789359, 836229–836230. For ESI and crystallographic data in CIF or other electronic format see DOI: 10.1039/c1sc00492a

polynuclear core can assemble.[13] Toward this end, we recently reported the synthesis of a new hexadentate ligand (MeC(CH_2NHPh-*o*-NH_2)$_3$) ($^{H}LH_6$)[14] that permits the isolation and characterization of well-defined trinuclear[14,15] and hexanuclear iron clusters.[16] The open-shell triiron complexes exhibit Fe–Fe bonding that is strengthened upon oxidation of the [Fe_3] core.[14] In addition, the seven-member electron-transfer series of Fe_6 clusters exhibits redox-dependent physical and chemical properties, which have been rationalized in terms of a qualitative molecular orbital model based on direct, yet relatively weak, Fe–Fe interactions.[16a] We were thus intrigued by the possibility of using structural perturbations to the hexamine ligand platform to tune the degree of metal–metal interactions and thus the electronic structure within the trinuclear core. Herein, we report the synthesis and characterization of a series of triiron complexes wherein the observed Fe–Fe separation is elongated relative to its Fe_3 predecessors, thereby giving rise to complexes featuring both intermediate- and high-spin electronic configurations. Furthermore, the electronic structure of the trinuclear complexes shows a strong dependence on the σ-donor strength of peripheral ligands employed, manifesting itself as changes in the observed spin ground states and temperature-induced changes in spin state. In light of the direct metal-orbital overlap found in this family of complexes, we propose the electronic and magnetic phenomena can be explained by considering the electronic population of a single molecular orbital manifold. The magnetic and spectroscopic data are reflective of this delocalized molecular electronic structure, dictated by simple ligand-field considerations, not individual metal centers within a cluster.

Results and discussion

Syntheses and structures

Standard Pd cross-coupling methodologies were used to install phenyl substituents onto the peripheral ligand amine groups of MeC(CH_2NHPh-*o*-NH_2)$_3$ ($^{H}LH_6$) using bromobenzene (3.1 equiv.) and sodium *tert*-butoxide base (4 equiv.), catalyzed by Pd_2(dba)$_3$/rac-BINAP (2.2%, 6.6%, respectively) in toluene (70 °C) for 18 h to afford MeC(CH_2NHPh-*o*-NHPh)$_3$ ($^{Ph}LH_6$, 80% isolated yield). The ligand could be efficiently isolated as a pale yellow solid following extraction of the crude reaction mixture with dichloromethane and washing the resultant solids with copious amounts of diethyl ether.

Metallation of the ligand platform was affected using iron-based organometallic or metal-amide starting materials. Reaction of $^{Ph}LH_6$ with 1.5 equivalents of $Fe_2(N(SiMe_3)_2)_4$ in a mixture of thawing diethyl ether and tetrahydrofuran (thf) afforded the stable, brown triiron complex (^{Ph}L)Fe_3(thf)$_3$ (**1**) in good overall yield (λ_{max}/nm (ε/(M^{-1} cm^{-1})): 428 (5800), 590 (2000 sh), 760 (1700); 60%, Scheme 1). Structural data are provided in Table 1. Complex **1** precipitated as an analytically pure, crystalline solid upon storage at −30 °C over a period of 12 h. A similar reaction of $^{Ph}LH_6$ with $Fe_2(Mes)_4$ in thawing thf with pyridine (3 equiv.) afforded the stable, brown pyridine-ligated complex (^{Ph}L)Fe_3(py)$_3$ (**2**) in good overall yield (λ_{max}/nm (ε/(M^{-1} cm^{-1})) 490 (6100); 66%). Complex **2** could be purified by precipitation from tetrahydrofuran or diethyl ether at −30 °C with excess pyridine present. The labile thf ligands in **1** can be readily exchanged for stronger σ-donating ligands. For example, reaction of **1** with five equivalents of dimethylphenylphosphine (PMe_2Ph) in a mixture of thf and diethyl ether results in formation of the tris-phosphine complex (^{Ph}L)Fe_3(PMe_2Ph)$_3$ (**3**) (λ_{max}/nm (ε/(M^{-1} cm^{-1})): 490 (6600), 730 (2300 sh); 65%).

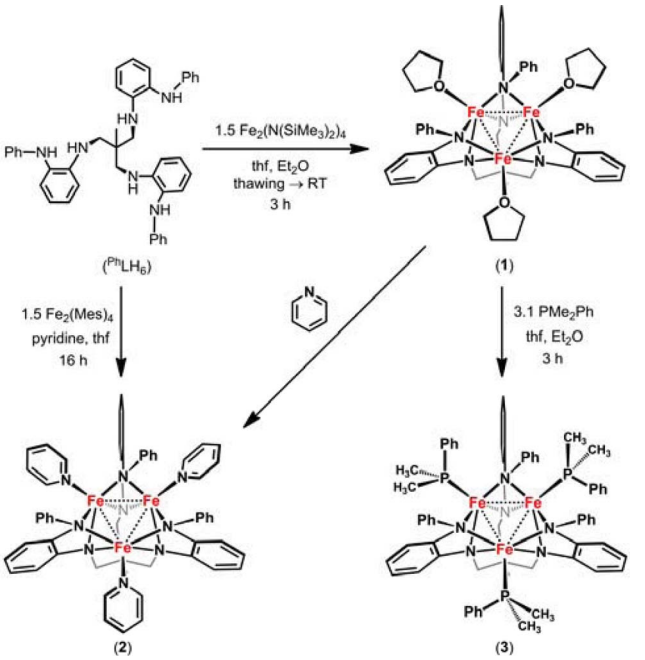

Scheme 1

Complex **1** was crystallized from a concentrated solution of benzene and hexanes at −30 °C, while concentrated benzene solutions of **2** and **3** stored at room temperature produced crystals suitable for X-ray diffraction analysis. The solid-state

Table 1 Selected core bond distances (Å) and angles (°) for **1**, **2** and **3**

Compound (L)	**1** (thf)	**2** (py)	**3** (PMe_2Ph)
Fe(1)–Fe(2)	2.4377(11)	2.6074(6)	2.5517(13)
Fe(1)–Fe(3)	2.5114(11)	2.5466(6)	2.5986(13)
Fe(2)–Fe(3)	2.5235(11)	2.5756(6)	2.6057(13)
Fe(1)–L(1)	2.151(4)	2.091(2)	2.479(2)
Fe(2)–L(2)	2.154(4)	2.115(2)	2.461(2)
Fe(3)–L(3)	2.101(4)	2.119(2)	2.397(2)
Fe(1)–N(2)	2.114(4)	2.193(2)	2.098(5)
Fe(1)–N(3)	2.169(5)	2.137(2)	2.099(5)
Fe(1)–N(5)	2.169(5)	2.109(2)	2.161(5)
Fe(1)–N(6)	2.204(4)	2.228(2)	2.265(5)
Fe(2)–N(1)	2.153(4)	2.208(2)	2.104(5)
Fe(2)–N(3)	2.142(4)	2.126(2)	2.204(5)
Fe(2)–N(4)	2.181(4)	2.128(2)	2.196(5)
Fe(2)–N(6)	2.146(4)	2.146(2)	2.108(5)
Fe(3)–N(1)	2.169(5)	2.078(2)	2.163(5)
Fe(3)–N(2)	2.203(5)	2.093(2)	2.158(5)
Fe(3)–N(4)	2.182(4)	2.269(2)	2.196(5)
Fe(3)–N(5)	2.176(5)	2.221(2)	2.212(5)
Fe2–N1–Fe3	71.44(14)	73.81(6)	75.24(16)
Fe1–N2–Fe3	71.11(14)	72.87(6)	75.24(15)
Fe1–N3–Fe2	68.86(13)	75.42(6)	72.69(15)
Fe2–N4–Fe3	70.68(13)	71.64(6)	73.27(15)
Fe1–N5–Fe3	70.61(15)	71.99(6)	72.91(15)
Fe1–N6–Fe2	68.14(13)	73.17(6)	71.29(15)

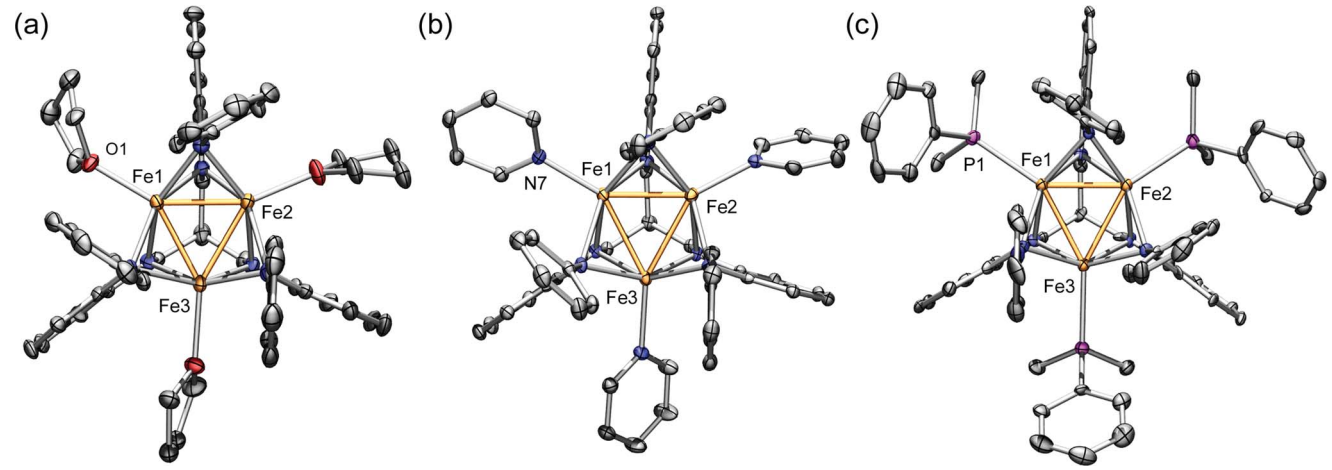

Fig. 1 Solid-state structures for **1** (a), **2** (b), and **3** (c), with thermal ellipsoids set at the 50% probability level. Orange, magenta, red, blue and gray ellipsoids represent Fe, P, O, N, and C, respectively; hydrogen atoms are omitted for clarity. Selected mean interatomic distances (Å) and angles (°) for **1**: Fe–Fe 2.491(1), Fe–N_{base} 2.158(5), Fe–N_{Ph} 2.176(5), Fe–O 2.135(4), Fe–N–Fe 70.14(15); **2**: Fe–Fe 2.576(1), Fe–N_{base} 2.139(2), Fe–N_{Ph} 2.183(2), Fe–N_{py} 2.108(2), Fe–N–Fe 73.15(6); **3**: Fe–Fe 2.585(2), Fe–N_{base} 2.138(6), Fe–N_{Ph} 2.190(6), Fe–P 2.446(2), Fe–N–Fe 73.44(16).

structures for the series are shown in Fig. 1. In all complexes **1–3**, each iron center resides in a distorted square pyramidal geometry, where four amide nitrogen atoms form a basal plane with an apical ligand (thf, py, or PMe_2Ph) *trans* to a di-iron unit. Each of the ligand η^2-amide residues bridge adjacent metal ions. The Fe–N bond distances to the base of the hexamide ligand (N_{base}) and diphenylamide crown (N_{Ph}) are consistent across the series (Fe–N_{base} (Å): **1** 2.158(5), **2** 2.139(3), **3** 2.138(6); Fe–N_{Ph} (Å): **1** 2.176 (5), **2** 2.183(3), **3** 2.190(6); selected bond distances are provided in Table 1) and substantially elongated in comparison to the (^{H}L)$Fe_3(PMe_2R)_3$ complexes (Fe–N_{base} 1.984(8); Fe–N_H 2.024(8) Å)[14] and related hexanuclear series $[(^{H}L)_2Fe_6(NCCH_3)_m]^{n+}$ (Fe–N_{ave} = 1.961(2)–2.067(3) Å).[16a] The bond metrics within each of the *o*-phenylenediamide (OPDA) branches are characteristic of being aromatic, closed-shell dianions (see Tables S4–6†) as opposed to other potential ligand oxidation states (*i.e.*, benzosemiquinonate diimine π-radical anion or neutral benzoquinone diimine).[17]

While the gross structural features and ligand connectivity of complexes **1–3** are similar to (^{H}L)$Fe_3(PMe_2R)_3$,[14] complexes **1–3** feature greater Fe–Fe separation (Å) than that observed in (^{H}L)$Fe_3(PMe_2R)_3$ (average Fe–Fe distance: 2.299(2) Å). Complex **1** features the shortest average Fe–Fe separation of 2.491(1) Å, followed by the pyridine complex **2** with 2.576(1) Å, and the phosphine complex **3** with 2.585(2) Å. The aryl substituents on the modified ligand (^{Ph}L) sterically prevent the Fe ions in **1–3** from getting as close as in (^{H}L)$Fe_3(PMe_2R)_3$, but the M–M separation is still within the range of reported Fe–Fe bonding interactions.[18]

Mössbauer spectroscopy

The zero-field ^{57}Fe Mössbauer spectrum of **1** shows a broad asymmetric quadrupole doublet at 105 K ((δ, $|\Delta E_Q|$ ($^{mm}/_{s}$)): 0.79, *1.25*, Γ_L = 0.52 $^{mm}/_{s}$, Γ_R = 0.43 $^{mm}/_{s}$, $\Gamma_{Fe\ foil}$ = 0.31 $^{mm}/_{s}$; see Fig. 2a). Analogous measurements on complexes **2** and **3** reveal the presence of two quadrupole doublets at 105 K and 110 K, respectively (see Fig. 2a, data summarized in Table 2). The major component in the spectrum for complex **2** features an isomer shift and quadrupole splitting (δ, $|\Delta E_Q|$ ($^{mm}/_{s}$): 0.82, *1.48*; 71%) similar to **1**, while the minor component features a larger quadrupole splitting (δ, $|\Delta E_Q|$ ($^{mm}/_{s}$): 0.85, *2.22*; 29%). The spectrum of complex **3** at 110 K is similar (major component 68%: δ, $|\Delta E_Q|$ ($^{mm}/_{s}$): 0.77, *1.43*; minor component 32%: δ, $|\Delta E_Q|$ ($^{mm}/_{s}$): 0.77, *2.30*). The spectral parameters are provided in Table 2. The Mössbauer parameters are consistent with a high-spin Fe^{II} electronic configuration, however the isomer shifts exceed other five-coordinate iron complexes featuring similar coordination spheres (four OPDA-based *N* and one *P*-donor) with lower spin-states.[17e,19] The isomer shifts for **1–3** are much higher than the low-spin (^{H}L)$Fe_3(PMe_2R)_3$ analogues (see Table 2), wherein extensive M–M bonding may substantially reduce shielding of the s-electron density at the iron nuclei, which may contribute to the decreased isomer shift.[20]

The presence of two quadrupole doublets for complexes **2** and **3** was probed further by obtaining the Mössbauer spectra at several temperatures. Spectra were collected for a sample of **2** in the temperature range 4–180 K (see Fig. 3, S12–16†) and for **3** in the range 80–250 K (see Fig. S17–21†). From 4–105 K, the spectrum for complex **2** exhibits two quadrupole doublets featuring nearly identical isomer shifts, but distinct splitting parameters (*i.e.*, **2** at 4 K, component 1 δ, $|\Delta E_Q|$ ($^{mm}/_{s}$): 0.83, *1.57*, 64%; component 2: 0.87, *2.76*, 36%; see Table S7† for compiled data over all temperature ranges). At 150 K and above, the two quadrupole doublets become less distinct (*i.e.*, **2** at 180 K, component 1 δ, $|\Delta E_Q|$ ($^{mm}/_{s}$): 0.78, *1.36*, 90%; component 2: 0.82, *1.66*, 10%). For complex **3**, the same phenomenon is observed: at and below 150 K two quadrupole doublets with nearly the same isomer shift are apparent (*i.e.*, **3** at 80 K, component 1 δ, $|\Delta E_Q|$ ($^{mm}/_{s}$): 0.78, *1.43*, 67%; component 2: 0.78, *2.43*, 33%), and for temperatures at and above 200 K, the hyperfine parameters for the two quadrupole doublets nearly converge (*i.e.*, **3** at 200 K, component 1 δ, $|\Delta E_Q|$ ($^{mm}/_{s}$): 0.73, *1.42*, 72%; component 2: 0.74, *1.81*, 28%). The data at each temperature have been therefore modeled using two quadrupole doublets (see Table S7†).

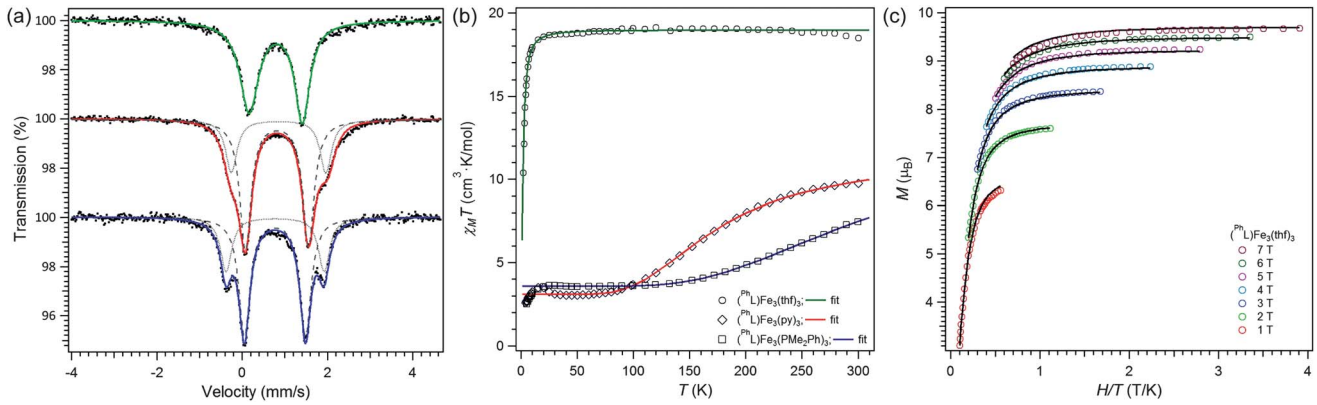

Fig. 2 (a) Zero-field ^{57}Fe Mössbauer spectra obtained for **1** (105 K; data black dots, spectral fit: green; δ, $|\Delta E_Q|$ ($^{mm}/_s$) 0.79, *1.25*); **2** (105 K; data black dots, spectral fit: red; δ, $|\Delta E_Q|$ ($^{mm}/_s$) 0.82, *1.48* (71%), 0.85, *2.22* (29%)), and **3** (110 K; data black dots, spectral fit: blue; δ, $|\Delta E_Q|$ ($^{mm}/_s$) 0.77, *1.43* (68%), 0.77, *2.30* (32%)). (b) Variable-temperature magnetic susceptibility data for **1** (circles), **2** (diamonds), and **3** (squares), collected in an applied dc field of 0.1 T. Solid lines represent fits to the data as described in the text. (c) Plot of reduced magnetization for **1** between 1.8 and 10 K at selected fields.

The isomer shifts for complex **1** and the contributing components in complexes **2** and **3** all fall within a very narrow range (*δ*: 0.7–0.87 $^{mm}/_s$). The presence of the two distinct quadrupole splitting parameters might correlate to molecular distortions present in the complexes or to a change in molecular spin states (see below). Support for a correlation to a structural distortion arises from the isosceles distortion featured by **1–3**. At the low-temperature extreme for **2**, the quadrupole doublets are in a nearly 2 : 1 ratio, consistent with the geometrically distinct sites manifesting a different electronic field gradient. Although all three sites are geometrically distinct in **1–3**, the similarity between the local geometries presumably gives rise to coincident spectral parameters, and thus only two quadrupole doublets are apparent. Indeed, a similar observation was observed in the Mössbauer spectra obtained for the related triiron compounds (NBu$_4$)[(^{tbs}L)Fe$_3$(μ^3-N)] and (^{tbs}L)Fe$_3$(μ^3-NCH$_3$).[15] Both of these compounds feature two quadrupole doublets with identical isomer shifts and differing quadrupole splitting parameters that coalesce to a single quadrupole doublet at elevated temperatures. In all of these cases, as the temperature increases, the iron nuclei within the complexes feel the same electronic charge distribution, giving rise to similar (or identical) isomer shift and quadrupole splitting parameters. Alternatively, the spectral changes observed in the Mössbauer may correlate to changes in the molecular spin state. This hypothesis is tested in the following section.

Magnetic properties

To probe the magnetic behavior of complexes **1–3**, variable-temperature dc susceptibility data were collected in the temperature range of 5–300 K. In the case of **1**, $\chi_M T$ remains relatively constant from 300 K down to 30 K, with an average value of $\chi_M T$ = 18.5 cm^3 K mol^{-1} (see Fig. 2b). Below 30 K, the data undergo a downturn, likely the result of Zeeman and zero-field splitting. The value of $\chi_M T$ = 18.5 cm^3 K mol^{-1} is much larger than the 9.00 cm^3 K mol^{-1} expected for three non-interacting high-spin Fe^{II} ions with g = 2.00, indicative of ferromagnetic coupling that persists even to 300 K. Indeed, the observed value is only slightly lower than the 21.0 cm^3 K mol^{-1} expected for an S = 6 ground state with g = 2.00. Accordingly, the data were modeled according to the following spin Hamiltonian given in eqn (1).

$$\hat{H} = -2J(\boldsymbol{S}_{Fe1}\boldsymbol{S}_{Fe2} + \boldsymbol{S}_{Fe2}\boldsymbol{S}_{Fe3} + \boldsymbol{S}_{Fe1}\boldsymbol{S}_{Fe3}) + D\boldsymbol{S}^2 + g\mu_B\boldsymbol{S}\cdot\boldsymbol{B} \quad (1)$$

The corresponding simulation using the program MAGPACK[21] that best reproduces the data affords parameters of $J \geq$

Table 2 Spectral and magnetic properties of complexes **1–3**

Compound	S	$\chi_M T$ (cm^3 K mol^{-1})	λ/nm (ε/M^{-1} cm^{-1})	δ ($^{mm}/_s$)	$\lvert\Delta E_Q\rvert$ ($^{mm}/_s$)	Γ ($^{mm}/_s$)^e	(%)
(^{Ph}L)Fe$_3$(thf)$_3$ (**1**)	6	18.38^a	428 (5800), 590 (2000, sh), 760, (1700)	0.79^f	1.25^f	0.52, 0.43	100
(^{Ph}L)Fe$_3$(py)$_3$ (**2**)	2	3.04^a (3.08)^b	490 (6100)	0.82^f	1.48^f	0.32, 0.32	71
				0.85	2.22	0.32, 0.32	29
	4	9.76^c (12.0)^d					
(^{Ph}L)Fe$_3$(PMe$_2$Ph)$_3$ (**3**)	2	3.58^a (3.58)^b	490 (6600), 730 (2300)	0.77^g	1.43^g	0.32, 0.32	68
				0.77	2.30	0.32, 0.32	32
	4	7.45^c (14.4)^d					
(^{H}L)Fe$_3$(PMe$_2$Ph)$_3$[14]	1	1.01^a	707 (900)	0.38	1.04	0.28, 0.28	100

^{a} Recorded at 40 K. ^{b} Obtained from fit as value for fully-populated S = 2 state. ^{c} Recorded at 300 K. ^{d} Obtained from fit as value for fully-populated S = 4 state. ^{e} Full width at half maximum for Lorentzian fits for low and high velocity peaks, respectively. ^{f} Recorded at 105 K. ^{g} 110 K.

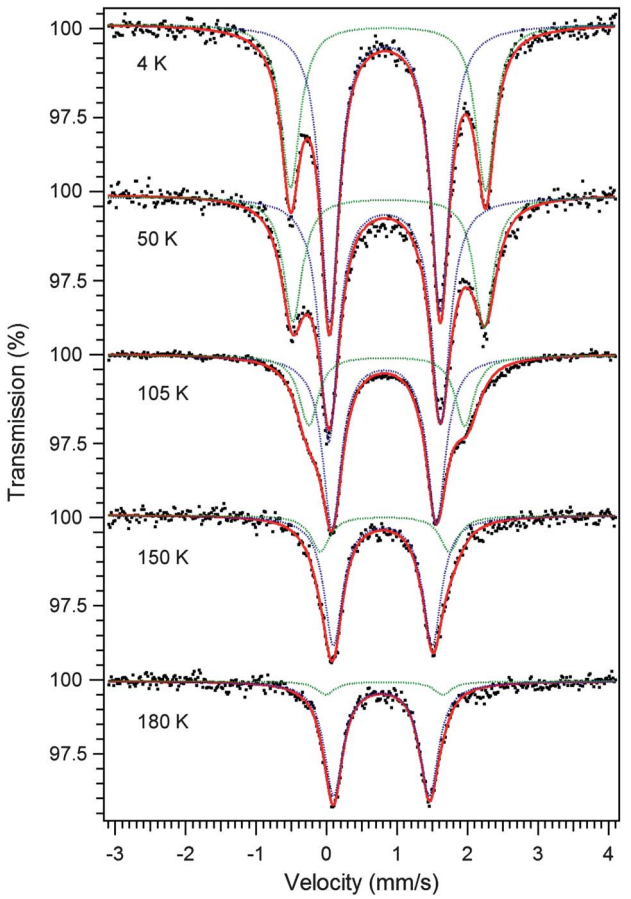

Fig. 3 Zero-field ^{57}Fe Mössbauer spectra obtained for **2** represented by black dots, spectral fit as solid red line (sum of components at variable temperatures) (δ, $|\Delta E_Q|$ ($^{mm}/_s$)): 4 K 0.83, *1.57* (64%), 0.87, *2.76* (36%); 50 K 0.83, *1.59* (65%), 0.88, *2.71* (35%); 105 K 0.82, *1.48* (71%), 0.85, *2.22* (29%); 150 K 0.80, *1.40* (78%), 0.83, *1.83* (22%); 180 K 0.78, *1.36* (90%), 0.82, *1.66* (10%).

+ 125 cm^{-1}, D = +3.5 cm^{-1}, and g = 1.88. Alternatively, the average value of $\chi_M T$ (18.5 cm^3 K mol^{-1}) for the temperature range 30–300 K may correspond to an $S = 5$ ground state with $g = 2.22$. Such a strong ferromagnetic interaction likely results from superexchange between Fe centers through the bridging amide ligands and/or direct exchange between Fe centers, as the average Fe–Fe separation of 2.491(1) Å is within the range of previously reported Fe–Fe bonding interactions.[18] The presence of such a high-spin ground state that remains isolated to 300 K is exceedingly rare in multinuclear clusters. In fact, evidence of the first example of an isolated $S = 6$ ground state was only very recently reported for the related cluster compounds (^{tbs}L)Fe_3(thf)[15] and (^{H}L)$_2Fe_6$.[16a] Among other single-valence complexes, we are not aware of examples exceeding $S = 4$, which has been observed in an Fe_4S_4 cubane cluster[22] and a diiron paddlewheel complex.[23] Finally, a number of dinuclear, Class III mixed-valence $[Fe_2]^V$ complexes have been shown to exhibit well-isolated $S = {}^9/_2$ ground states that arise from electron delocalization *via* a double-exchange mechanism.[6a,24]

To further probe the spin ground state and downturn of $\chi_M T$ at low temperature, variable-temperature magnetization data were collected in the temperature range 1.8–10 K at fields of 1 to 7 T. The resulting plot of reduced magnetization, shown in Fig. 2c, features a series of non-superimposable isofield curves, with the 7 T curve reaching a maximum value of $M = 9.7$ μ_B at 1.8 K. While this value falls short of the 12.0 μ_B expected for an $S = 6$ ground state, the non-superimposability of the isofield curves demonstrates that significant magnetic anisotropy is precluding saturation of the magnetization. To quantify this effect, the data were modeled according to the Hamiltonian given in eqn (2).

$$\hat{H} = D\hat{S}_z^2 + E(\hat{S}_x^2 - \hat{S}_y^2) + g\mu_B \boldsymbol{S}\cdot\boldsymbol{B} \quad (2)$$

The corresponding fit to the data, obtained using ANISOFIT 2.0[25] and considering an $S = 6$ ground state, provides axial and transverse zero-field splitting parameters of D = +1.3 cm^{-1} and $|E| = 0.2$ cm^{-1}, respectively, with $g = 1.9$. Note that a fit of similar quality can be obtained for an $S = 5$ ground state, giving values of D = +1.7 cm^{-1}, $|E| = 0.3$ cm^{-1}, and $g = 2.3$ (see Fig. S24†).

In sharp contrast to the temperature-independent magnetic susceptibility observed for **1**, the $\chi_M T$ *vs.* T data for **2** undergo a gradual decline from 9.76 cm^3 K mol^{-1} at 300 K to 3.04 cm^3 K mol^{-1} at 40 K (see Fig. 2b). At 300 K, the value of $\chi_M T$ is reasonably close to the expected value of 9.00 for three non-interacting Fe^{II} ions with $g = 2.00$. In addition, the value at 40 K is close to the value of 3.00 expected for an $S = 2$ state. This behavior was initially interpreted as resulting from antiferromagnetic superexchange between Fe^{II} centers through the bridging amide ligands. As such, the data were first modeled according to the following spin Hamiltonian for an equilateral triangle of Fe^{II} centers given in eqn (1). However, using MAGPACK, this model failed to reproduce the data (see Fig. S27†). As such, the following two alternative models were also employed, considering isosceles (2 independent J values) and scalar (3 independent J values) triangles, respectively:

$$\hat{H} = -2[J_1(\boldsymbol{S}_{Fe1}\boldsymbol{S}_{Fe2} + \boldsymbol{S}_{Fe2}\boldsymbol{S}_{Fe3}) + J_2\boldsymbol{S}_{Fe1}\boldsymbol{S}_{Fe3}] + D\boldsymbol{S}^2 + g\mu_B\boldsymbol{S}\cdot\boldsymbol{B} \quad (3)$$

$$\hat{H} = -2(J_1\boldsymbol{S}_{Fe1}\boldsymbol{S}_{Fe2} + J_2\boldsymbol{S}_{Fe2}\boldsymbol{S}_{Fe3} + J_3\boldsymbol{S}_{Fe1}\boldsymbol{S}_{Fe3}) + D\boldsymbol{S}^2 + g\mu_B\boldsymbol{S}\cdot\boldsymbol{B} \quad (4)$$

Still, neither of these models, despite the introduction of additional parameters, succeeded to reproduce the data (see Fig. S28–29†). Qualitative inspection of the data along with various simulations reveals the incompatibility of the high- and low-temperature regimes when considering a simple superexchange mechanism. Indeed, in order for the exchange interaction to be strong enough to provide ground state isolation at 40 K for **2**, the value of $\chi_M T$ at 300 K must be much lower than that observed. Furthermore, a shift from ferromagnetic superexchange in compound **1** to antiferromagnetic superexchange in compound **2** would likely be dictated by Fe–N–Fe angle. However, the mean Fe–N–Fe angle changes only from 70.14(15)° in **1** to 73.15(6)° in **2** and 73.44(15)° in **3** (see Table 1). While dramatic magnetostructural correlation is not uncommon in dinuclear Cu^{II}–X–Cu^{II} (X = O, OH, Cl, Br) linkages, where the nature and magnitude of superexchange is dictated by Cu–X-Cu angle and the electronic properties of other ancillary ligands,[26] we are unaware of such pronounced magnetostructural dependence among iron(II) centers. Moreover, an $S = 6$ ground state,

isolated at 300 K, has been observed in the related cluster (^{tbs}L)Fe_3(thf),[15] which features an even larger mean Fe–N–Fe angle of 77.95(8)°.[15] Thus, it is unlikely that the exchange in the Fe_3 core would shift from ferromagnetic to antiferromagnetic, then back to ferromagnetic, with increasing Fe–N–Fe angle.

Another possible explanation of the temperature-dependent behavior of **2** is site-isolated spin crossover of the individual Fe^{II} centers.[27] However, spin crossover is typically accompanied by diagnostic spectroscopic and structural changes, where ferrous ions, in particular, exhibit substantial changes in the observed isomer shift and quadrupole splitting in the Mössbauer spectrum.[27a,b,d] While two quadrupole doublets are apparent in the Mössbauer spectra of **2** at temperatures below 105 K the isomer shifts for both contributing components are nearly identical in all cases and very similar for all three complexes studied. Moreover, large structural changes typically accompany Fe^{II} centers undergoing a spin crossover as the electronic configuration changes from low-spin to high-spin.[27,28] Yet, variable-temperature X-ray diffraction on a single crystal of **2** does not show evidence for any structural changes in the temperature range of 100–300 K in 50 K increments (see Fig. S3–8†), further suggesting the individual Fe ions in **2** are not undergoing site-isolated spin crossover. The overlay of the molecular structure obtained for **2** at 100 K and 300 K is displayed in Fig. 4. Notably, the local iron coordination environments, the bond metrics within the triiron core, and the gross structural features for the molecule as a whole are preserved over the temperature range investigated.

Since superexchange through the amide bridges or site-isolated spin crossover do not provide satisfactory models for the magnetic behavior of **2**, we consider a thermal equilibrium between an $S = 2$ ground state and a single excited spin state. Indeed, while the value of $\chi_M T = 9.76$ cm^3 K mol^{-1} at 300 K is close to the 9.00 expected for three isolated high-spin Fe^{II} ions, it is even closer to the expected value of 10.0 for a single, $S = 4$ spin state. Here, the Fe_3 core can be considered as a single spin unit, arising from a delocalized core electronic structure. Along these lines, recent spectroscopic and magnetic analysis have provided evidence for a similar phenomenon in the related clusters $[(^{H}L)_2Fe_6(NCMe)_m]^{n+}$ ($m = 0, 2, 4, 6$; $n = -1, 0, 1, 2, 3, 4, 6$).[16a,b] To quantitatively probe the possibility of a delocalized spin equilibrium, the $\chi_M T$ data were modeled from 40–300 K considering a simple Boltzmann population (see Fig. 2b) of the two states, according to the following expressions:

$$x = 1/(1 + \exp[(\Delta H/R)(1/T - 1/T_C)]) \quad (5)$$

$$x = (\chi T - (\chi T)_{LS})/((\chi T)_{HS} - (\chi T)_{LS}) \quad (6)$$

where x is the molar fraction of high-spin (in this case $S = 4$) molecules, ΔH is the change in enthalpy associated with the spin state transition, R is the molar gas constant, and T_c is the critical temperature.[29] Indeed, this treatment leads to an excellent fit of the data, providing estimates of thermodynamic parameters of $\Delta H = 406$ cm^{-1} and $T_c = 187$ K. The fit for **2** corresponds to $\chi_M T_{LS} = 3.08$ cm^3 K mol^{-1} ($g_{LS} = 2.03$) and $\chi_M T_{HS} = 12.0$ cm^3 K mol^{-1} ($g_{HS} = 2.19$). The population of lower S values in **2**, in contrast to the well-isolated $S = 6$ state in **1**, is likely a direct result of stronger field pyridine *versus* thf ancillary ligands (see below). The observation of a delocalized spin state equilibrium here is reminiscent of a class of mixed-valence dinuclear $[Ru_2]^{5+}$ species.[30] In these species, variable-temperature magnetic susceptibility data indicated a thermally-induced transition from an $S = {}^1/_2$ state to an $S = {}^3/_2$ ground state. In addition, a similar $S = {}^1/_2 \leftrightarrows S = {}^3/_2$ equilibrium was recently reported in the dinitrogen-bridged, mixed-valence dichromium complex $[(dmpe)_4Cr^{I}Cr^{II}(C_2Si^{i}Pr_3)_2(\mu\text{-}N_2)]^+$.[31] Regarding examples of trinuclear clusters exhibiting such a phenomenon, a family of linear Co_3 complexes was shown to display transitions between both integer[32] and non-integer[33] spin states, depending on oxidation state. Finally, trigonal trinuclear Co and mixed Co/Rh complexes featuring carbonyl or chalcogenide capped trinuclear cores have been shown to feature thermally induced spin state changes analogous to those reported here.[34]

In order to confirm the $S = 2$ ground state in **2**, low-temperature magnetization data were collected. The corresponding plot of reduced magnetization displays a set of non-superimposable isofield curves, with a maximum value of $M = 2.6$ μ_B at 7 T and 1.8 K (see Fig. S30†). When treated with the Hamiltonian in eqn (2) and ANISOFIT 2.0, the data are modeled well in the temperature range 3–10 K for an $S = 2$ ground state, providing parameters of $D = +14.7$ cm^{-1}, $|E| = 4.0$ cm^{-1}, and $g = 2.2$. Note that at temperatures below 3 K, especially at low fields, the data undergo a slight downturn, possibly stemming from weak intermolecular interactions between neighboring clusters.

The plot of $\chi_M T$ *vs.* T for compound **3** exhibits a profile similar to that of **2**, albeit with the transition shifted to higher temperature (see Fig. 2b).[35] Indeed, as the temperature is decreased, $\chi_M T$ undergoes a gradual decline from 7.45 cm^3 K mol^{-1} at 300 K to a plateau of 3.58 cm^3 K mol^{-1} below 100 K. The data for **3** can be treated analogously to those for **2**, according to eqn (5) and (6), to give parameters of $\Delta H = 604$ cm^{-1} and $T_c = 375$ K. The fit for **3** corresponds to $\chi_M T_{LS} = 3.58$ cm^3 K mol^{-1} ($g_{LS} = 2.19$) and $\chi_M T_{HS} = 14.4$ cm^3 K mol^{-1} ($g_{HS} = 2.40$). Here, the substantial increase in transition temperature when moving from **2** to **3** is consistent with replacing pyridine ligands with stronger field phosphine ligands (see below).

Low-temperature magnetization data, collected for compound **3** in the temperature range 3–10 K, are very similar to those for compound **2** (see Fig. S36†). Indeed, a plot of reduced magnetization reveals a set of non-superimposable isofield curves, with

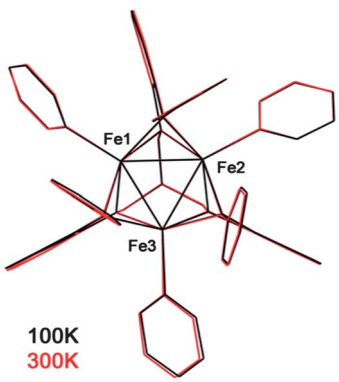

Fig. 4 Overlay of the X-ray crystal structure for **2** obtained at 100 K (black) and 300 K (red).

the magnetization reaching a maximum of $M = 3.1\ \mu_B$ at 7 T and 1.8 K. Accordingly, the data can be fit considering an $S = 2$ ground state to give parameters of $D = +8.5\ cm^{-1}$, $|E| = 2.0\ cm^{-1}$, and $g = 2.2$. Finally, below 3 K, the data undergo a slight downturn, akin to that observed for compound **2**.

Attempts to correlate the change in molecular spin state with the change in observed Mössbauer parameters for complexes **2** and **3** have thus far been unsuccessful. The convergence of the two quadrupole doublets into a single quadrupole doublet does not manifest at the same temperatures where the spin state change occurs. For both complexes the quadrupole splitting parameters have significantly converged before a substantial fraction of the $S = 4$ state should be present. For example, the Mössbauer spectrum of **3** at 150 K shows nearly superimposed quardrupole doublets (Fig. S19†), whereas the susceptibility data indicate the majority of the material should remain in the ground state (Fig. 2b). Furthermore, attempts to reproduce the data using a relaxation model[36] failed to yield physically reasonable parameters (see ESI for details†).

Qualitative electronic structure

The above analysis, based on magnetic, crystallographic, and Mössbauer spectral data, provides strong evidence that the observed behavior of the Fe_3 clusters cannot be attributed simply to superexchange through bridging amide ligands or site-isolated spin crossover. As such, we turn our attention to the possibility that the phenomena can be explained according to a simple qualitative molecular orbital scheme, where iron–iron interactions within the core give rise to a set of frontier orbitals comprised of 3d orbitals. This approach is derived following Cotton's method of describing metal–metal bonding interactions in $[Re_3Cl_9(\mu^2\text{-}Cl)_3]^{3-}$,[37] which has also been applied to describe the M–M interactions within $(^{H}L)Fe_3(PMe_2R)_3$.[14] In addition, we recently presented a similar model, closely following previous work with octahedral M_6 clusters,[37,38] to rationalize the redox-dependent properties of an electron-transfer series of octahedral Fe_6 clusters.[16a] Mixing the frontier orbitals of the three iron centers produces six bonding (4e features M–M σ bonding overlap with M–N σ* character), three non-bonding, and six anti-bonding molecular orbital combinations with respect to the M–M interactions, qualitatively illustrated in Fig. 5. For a trinuclear all-ferrous cluster, populating the 15 frontier d-orbitals with 18 valence electrons gives rise to possible spin states from $S = 0$ to $S = 6$. The combination of the weak-field bridging amide ligands and the weak-field thf ligands likely engenders the high-spin, $S = 6$ ground state in **1**. Here, the high-spin electronic configuration for **1** results from populating all available orbitals, even the highest-energy $2a_2$ (σ_{Fe-N}*) orbitals. Note, however, that the possibility of an $S = 5$ ground state, as suggested by fits to reduced magnetization data as an alternative configuration, could exist given a substantial energetic separation between the $1a_2$ and $2a_2$ orbitals.

Moving from compound **1** to compound **2**, the three ancillary thf ligands are replaced by pyridine ligands. The stronger ligand field imposed by the pyridine ligands should most significantly modulate the relative energies of Fe_3 core orbitals with d_z^2 character, as those orbitals can engage in σ interactions with the ancillary ligand p_z orbitals. Specifically, these interactions are

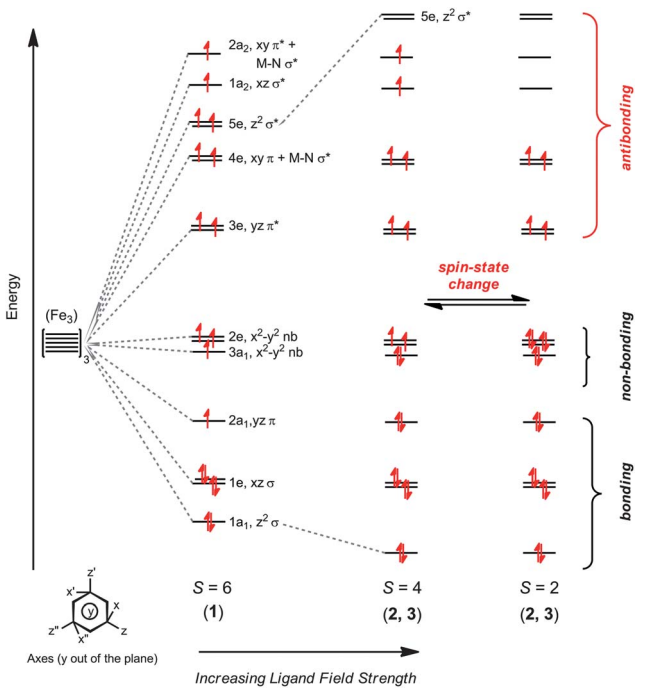

Fig. 5 Molecular orbital representation of the 3d orbital manifold for the trinuclear Fe complexes. Increasing the ancillary ligand strength increases the energy of the 5e orbital set, making thermal population of the $S = 6$ spin state inaccessible.

expected to lower the energy of the $1a_1$ bonding molecular orbital, while raising the energy of the 5e antibonding orbitals. Indeed, the energetic increase of the 5e orbital set is consistent with the lower spin ground state of **2** compared to **1**, where population of the $S = 6$ spin state is not inaccessible. Based on this rationale, **3** would be expected to exhibit similar behavior, as the even stronger-field phosphine ligands would lead to a further lowering of the $1a_1$ and raising of the 5e orbitals. Notably, though, perturbation of the d_z^2-based orbitals alone does not explain the difference in T_c observed between **2** and **3**. Possibly, π-type interactions would need to be considered to rationalize this discrepancy, however, we limit our orbital treatment to σ-interactions in order to avoid overcomplication of a simple and rudimentary model.

Conclusions and outlook

The development of polynuclear coordination complexes in our laboratory was intended to give rise to well-defined molecules with greater redox-flexibility and tunable electronic structure. Triiron complexes have now been observed spanning five distinct spin states: $S = 1$, $^3/_2$, 2, 4, and 6.[14,15] Thus it is possible to stabilize polynuclear, open-shell clusters, whose direct M–M interactions give rise to electronic configurations suggestive of delocalized bonding maintained across the spin state series. The magnetic data and Mössbauer spectra obtained for these complexes are reflective of this delocalized *molecular* electronic structure, not *individual* metal centers within a cluster. In principle, similar open-shell electronic configurations could be realized for other polynuclear complexes, encompassing other

transition metal ions and with higher nuclearity. Research is currently underway to probe these possibilities and to determine how the electronic structure of polynuclear complexes changes when undergoing redox chemistry.

Acknowledgements

The authors thank Harvard University for financial support and Prof. R. H. Holm for the generous use of his Mössbauer spectrometer. E.V.E. thanks the HUCE Graduate Consortium for support.

Notes and references

1 (*a*) T. Mallah, S. Thiebaut, M. Verdaguer and P. Veillet, *Science*, 1993, **262**, 1554; (*b*) S. Ferlay, T. Mallah, R. Ouhes, P. Veillet and M. Verdaguer, *Nature*, 1995, **378**, 701; (*c*) O. Hatlevik, W. E. Buschmann, J. Zhang, J. L. Manson and J. S. Miller, *Adv. Mater.*, 1999, **11**, 914; (*d*) S. M. Holmes and G. S. Girolami, *J. Am. Chem. Soc.*, 1999, **121**, 5593; (*e*) S. S. Kaye, H. J. Choi and J. R. Long, *J. Am. Chem. Soc.*, 2008, **130**, 16921; (*f*) P. Dechambenoit and J. R. Long, *Chem. Eur. J.*, 2011, **40**, 3249 and references therein.

2 (*a*) R. Sessoli, H. L. Tsai, A. R. Schake, S. Wang, J. B. Vincent, K. Folting, D. Gatteschi, G. Christou and D. N. Hendrickson, *J. Am. Chem. Soc.*, 1993, **115**, 1804; (*b*) R. Sessoli, D. Gatteschi, A. Caneschi and M. A. Novak, *Nature*, 1993, **365**, 141; (*c*) D. Gatteschi, R. Sessoli, and J. Villain, *Molecular Nanomagnets*; Oxford University Press: New York, 2006, and references therein; (*d*) C. J. Milios, A. Vinslava, W. Wernsdorfer, S. Moggach, S. Parsons, S. P. Perlepes, G. Christou and E. K. Brechin, *J. Am. Chem. Soc.*, 2007, **129**, 2754; (*e*) D. Yoshihara, S. Karasawa and N. Koga, *J. Am. Chem. Soc.*, 2008, **130**, 10460; (*f*) D. E. Freedman, D. M. Jenkins, A. T. Iavarone and J. R. Long, *J. Am. Chem. Soc.*, 2008, **130**, 2884.

3 (*a*) A. Caneschi, D. Gatteschi, N. Lalioti, C. Sangregorio, R. Sessoli, G. Venturi, A. Vindigni, A. Rettori, M. G. Pini and M. A. Novak, *Angew. Chem., Int. Ed.*, 2001, **40**, 1760; (*b*) R. Clérac, H. Miyasaka, M. Yamashita and C. Coulon, *J. Am. Chem. Soc.*, 2002, **124**, 12837; (*c*) R. Lescouëzec, J. Vaissermann, C. Ruiz-Pérez, F. Lloret, R. Carrasco, M. Julve, M. Verdaguer, Y. Dromzée, D. Gatteschi and W. Wernsdorfer, *Angew. Chem., Int. Ed.*, 2003, **42**, 1483; (*d*) T. F. Liu, D. Fu, S. Gao, Y. Z. Zhang, H. L. Sun, G. Su and Y. J. Liu, *J. Am. Chem. Soc.*, 2003, **125**, 13976; (*e*) C. Coulon, H. Miyasaka and R. Clérac, *Struct. Bonding*, 2006, **122**, 163; (*f*) K. Bernot, L. Bogani, A. Caneschi, D. Gatteschi and R. Sessoli, *J. Am. Chem. Soc.*, 2006, **128**, 7947; (*g*) H. Miyasaka, M. Julve, M. Yamashita and R. Clérac, *Inorg. Chem.*, 2009, **48**, 3420 and references therein; (*h*) T. D. Harris, M. V. Bennett, R. Clérac and J. R. Long, *J. Am. Chem. Soc.*, 2010, **132**, 3980.

4 (*a*) R. Clerac, F. A. Cotton, K. R. Dunbar, C. A. Murillo, I. Pascual and X. Wang, *Inorg. Chem.*, 1999, **38**, 2655; (*b*) J. F. Berry, F. A. Cotton, T. Lu, C. A. Murillo, B. K. Roberts and X. Wang, *J. Am. Chem. Soc.*, 2004, **126**, 7082; (*c*) J. F. Berry, F. A. Cotton, T. Lu, C. A. Murillo, B. K. Roberts and X. Wang, *J. Am. Chem. Soc.*, 2004, **126**, 7082; (*d*) J. F. Berry, *Struct. Bonding*, 2010, **136**, 1 and references therein.

5 (*a*) N. S. Hush, *Prog. Inorg. Chem.*, 1967, **8**, 391; (*b*) C. Creutz, *Prog. Inorg. Chem.*, 1983, **30**, 1; (*c*) K. D. Demadis, C. M. Hartshorn and T. J. Meyer, *Chem. Rev.*, 2001, **101**, 2655; (*d*) B. S. Brunschwig, C. Creutz and N. Sutin, *Chem. Soc. Rev.*, 2002, **31**, 168; (*e*) D. M. D'Alessandro and F. R. Keene, *Chem. Soc. Rev.*, 2006, **35**, 424.

6 (*a*) S. Drüeke, P. Chaudhuri, K. Pohl, K. Wieghardt, X.-Q. Ding, E. Bill, A. Sawaryn, A. X. Trautwein, H. Winkler and S. J. Gurman, *Chem. Commun.*, 1989, 59; (*b*) T. Beissel, F. Birkelbach, E. Bill, T. Glaser, F. Kesting, C. Krebs, T. Weyhermüller, K. Wieghardt, C. Butzlaff and A. X. Trautwein, *J. Am. Chem. Soc.*, 1996, **118**, 12376; (*c*) M. P. Shores and J. R. Long, *J. Am. Chem. Soc.*, 2002, **124**, 3512; (*d*) B. Bechlars, D. M. D'Alessandro, D. M. Jenkins, A. T. Iavarone, S. D. Glover, C. P. Kubiak and J. R. Long, *Nat. Chem.*, 2010, **2**, 362.

7 I. I. Chernyaev, E. V. Shenderetskaya and A. A. Koryagina, *Zh. Neorg. Khim.*, 1960, **5**, 1163.

8 (*a*) F. A. Cotton, N. F. Curtis, C. B. Harris, B. F. G. Johnson, S. J. Lippard, J. T. Mague, W. R. Robinson and J. S. Wood, *Science*, 1964, **145**, 1305; (*b*) F. A. Cotton and R. A. Walton, *Multiple Bonds Between Metal Atoms*, Oxford (Oxford), 1993.

9 T. Nguyen, A. D. Sutton, M. Brynda, J. C. Fettinger, G. J. Long and P. P. Power, *Science*, 2005, **310**, 844.

10 (*a*) F. A. Cotton, *Acc. Chem. Res.*, 1978, **11**, 225; (*b*) *Multiple Bonds Between Metal Atoms*, ed. F. A. Cotton, C. A. Murillo and R. A. Walton, 3rd edn, Springer Science, New York, 2005, pp. 447–451.

11 F. A. Cotton, *Acc. Chem. Res.*, 1969, **2**, 240.

12 (*a*) P. Venkateswara Rao and R. H. Holm, *Chem. Rev.*, 2004, **104**, 527; (*b*) S. C. Lee and R. H. Holm, *Chem. Rev.*, 2004, **104**, 1135; (*c*) M. Shatruk, C. Avendano, and K. Dunbar, in *Progress in Inorganic Chemistry*, ed. K. D. Karlin, John Wiley & Sons, Amsterdam, 2009, vol. 56, pp. 155.

13 (*a*) P. E. Baikie and O. S. Mills, *Inorg. Chim. Acta*, 1967, **1**, 55; (*b*) H. Kisch, P. Reisser and F. Knoch, *Chem. Ber.*, 1991, **124**, 1143; (*c*) A. L. Keen, M. Doster, H. Han and S. A. Johnson, *Chem. Commun.*, 2006, 1221; (*d*) J. A. Hatnean, R. Raturi, J. Lefebvre, D. B. Leznoff, G. Lawes and S. A. Johnson, *J. Am. Chem. Soc.*, 2006, **128**, 14992; (*e*) E. C. Brown, B. Johnson, S. Palavicini, B. E. Kucera, L. Casella and W. B. Tolman, *Dalton Trans.*, 2007, 3035; (*f*) E. Y. Tsui, M. W. Day and T. Agapie, *Angew. Chem., Int. Ed.*, 2011, **50**, 1668.

14 Q. Zhao and T. A. Betley, *Angew. Chem., Int. Ed.*, 2011, **50**, 709.

15 (*a*) T. M. Powers, A. R. Fout, S.-L. Zheng and T. A. Betley, *J. Am. Chem. Soc.*, 2011, **133**, 3336; (*b*) T. M. Powers, and T. A. Betley, Unpublished results.

16 (*a*) Q. Zhao, T. D. Harris and T. A. Betley, *J. Am. Chem. Soc.*, 2011, **133**, 8293; (*b*) T. D. Harris, Q. Zhao, R. Hernández Sánchez and T. A. Betley, *Chem. Commun.*, 2011, **47**, 6344; (*c*) T. D. Harris and T. A. Betley, *J. Am. Chem. Soc.*, 2011, **133**, 13852.

17 (*a*) A. L. Balch and R. H. Holm, *J. Am. Chem. Soc.*, 1966, **88**, 5201; (*b*) L. F. Warren, *Inorg. Chem.*, 1977, **16**, 2814; (*c*) A. Anillo, M. R. Diaz, S. Garcia-Granda, R. Obeso-Rosete, A. Galindo, A. Ienco and C. Mealli, *Organometallics*, 2004, **23**, 471; (*d*) E. Bill, E. Bothe, P. Chaudhuri, K. Chlopek, K. Herebian, S. Kokatam, K. Ray, T. Weyhermüller, F. Neese and K. Wieghardt, *Chem.–Eur. J.*, 2005, **11**, 204; (*e*) K. Chlopek, E. Bill, T. Weyhermüller and K. Wieghardt, *Inorg. Chem.*, 2005, **44**, 7087.

18 (*a*) E. J. Wucherer, M. Tasi, B. Hansert, A. K. Powell, M.-T. Garland, J.-F. Halet, J.-Y. Saillard and H. Vahrenkamp, *Inorg. Chem.*, 1989, **28**, 3564; (*b*) H.-R. Gao, T. C. W. Mak, B.-S. Kang, B.-M. Wu, Y.-J. Xu, Y.-X. Tong and X.-L. Yu, *J. Chem. Res. S.*, 1996, **5**, 186; (*c*) M. Kim and J. Han, *Polyhedron*, 2007, **26**, 2949; (*d*) C. R. Hess, T. Weyhermüller, E. Bill and K. Wieghardt, *Angew. Chem., Int. Ed.*, 2009, **48**, 3703.

19 S. C. Bart, E. Lobkovsky, E. Bill, K. Wieghardt and P. Chirik, *Inorg. Chem.*, 2007, **46**, 7055.

20 R. E. Watson and A. J. Freeman, *Phys. Rev.*, 1960, **120**, 1125.

21 J. J. Borrás-Almenar, J. M. Clemente-Juan, E. Coronado and B. S. Tsukerblat, *J. Comput. Chem.*, 2001, **22**, 985.

22 M. Chakrabarti, L. Deng, R. H. Holm, E. Münck and E. L. Bominaar, *Inorg. Chem.*, 2009, **48**, 2735.

23 F. A. Cotton, L. M. Daniels, J. H. Matonic and C. A. Murillo, *Inorg. Chim. Acta*, 1997, **256**, 277.

24 (*a*) X.-Q. Ding, E. L. Bominaar, E. Bill, H. Winkler, A. X. Trautwein, S. Drüeke, P. Chaudhuri and K. Wieghardt, *J. Chem. Phys.*, 1990, **92**, 178; (*b*) S. K. Dutta, J. Ensling, R. Werner, U. Flörke, W. Haase, P. Gütlich and K. Nag, *Angew. Chem., Int. Ed.*, 1997, **36**, 152; (*c*) D. D. LeCloux, R. Davydov and S. J. Lippard, *J. Am. Chem. Soc.*, 1998, **120**, 6810; (*d*) D. Lee, C. Krebs, B. H. Huynh, M. Hendrich and S. J. Lippard, *J. Am. Chem. Soc.*, 2000, **122**, 5000; (*e*) S. Hazra, S. Sasmal, M. Fleck, F. Grandjean, M. T. Sougrati, M. Ghosh, T. D. Harris, P. Bonville, G. J. Long and S. Mohanta, *J. Chem. Phys.*, 2011, **134**, 174507.

25 M. P. Shores, J. J. Sokol and J. R. Long, *J. Am. Chem. Soc.*, 2002, **124**, 2279.

26 (*a*) D. J. Hodgson, *Prog. Inorg. Chem.*, 1975, **19**, 173 and references therein; (*b*) W. E. Hatfield, in *Magnetostructural Correlations in Exchange Coupled Systems*, ed. R. D. Willett and D. Gatteschi, NATO ASI Series, Reidel, Dordrecht, 1985.

27 (*a*) J. A. Real, I. Castro, A. Bousseksou, M. Verdaguer, R. Burriel, M. Castro, J. Linares and F. Varret, *Inorg. Chem.*, 1997, **36**, 455; (*b*) J.-F. Létard, J. A. Real, N. Moliner, A. B. Gaspar, L. Capes, O. Cador and O. Kahn, *J. Am. Chem. Soc.*, 1999, **121**, 10630; (*c*) N. Moliner, M. C. Muńoz, J.-F. Létard, L. Salmon, J.-P. Tuchagues, A. Bousseksou and J. A. Real, *Inorg. Chem.*, 2002, **41**, 6997; (*d*) M. Shatruk, A. Dragulescu-Andrasi, K. E. Chambers, S. A. Stoian, E. L. Bominaar, C. Achim and K. R. Dunbar, *J. Am. Chem. Soc.*, 2007, **129**, 6104.
28 S. Alvarez, *J. Am. Chem. Soc.*, 2003, **125**, 6795.
29 O. Kahn, *Molecular Magnetism*; VCH, New York, 1993.
30 (*a*) M. J. Bennett, K. G. Caulton and F. A. Cotton, *Inorg. Chem.*, 1969, **8**, 1; (*b*) P. Angaridis, F. A. Cotton, C. A. Murillo, D. Villagrán and X. Wang, *J. Am. Chem. Soc.*, 2005, **127**, 5008; (*c*) M. C. Barral, T. Gallo, S. Herrero, R. Jiménez-Aparicio, M. R. Torres and F. A. Urbanos, *Inorg. Chem.*, 2006, **45**, 3639; (*d*) M. C. Barral, T. Gallo, S. Herrero, R. Jiménez-Aparicio, M. R. Torres and F. A. Urbanos, *Chem.–Eur. J.*, 2007, **13**, 10088.
31 W. A. Hoffert, A. K. Rappé and M. P. Shores, *Inorg. Chem.*, 2010, **49**, 9497.
32 R. Clérac, F. A. Cotton, K. R. Dunbar, T. Lu, C. A. Murillo and X. Wang, *J. Am. Chem. Soc.*, 2000, **122**, 2272.
33 (*a*) F. A. Cotton, C. A. Murillo and X. Wang, *Inorg. Chem.*, 1999, **38**, 6294; (*b*) R. Clérac, F. A. Cotton, K. R. Dunbar, T. Lu, C. A. Murillo and X. Wang, *Inorg. Chem.*, 2000, **39**, 3065; (*c*) R. Clérac, F. A. Cotton, L. M. Daniels, K. R. Dunbar, K. Kirschbaum, C. A. Murillo, A. A. Pinkerton, A. J. Schultz and X. Wang, *J. Am. Chem. Soc.*, 2000, **122**, 6226; (*d*) R. Clérac, F. A. Cotton, L. M. Daniels, K. R. Dunbar, C. A. Murillo and X. Wang, *Inorg. Chem.*, 2001, **40**, 1256.
34 (*a*) S. Otsuka, A. Nakamura and T. Yoshida, *Inorg. Chem.*, 1968, **7**, 261; (*b*) M. Sorai, A. Kosaki, H. Suga, S. Seki, T. Yoshida and S. Otsuka, *Bull. Chem. Soc. Jpn.*, 1971, **44**, 2364; (*c*) P. D. Frisch and L. F. Dahl, *J. Am. Chem. Soc.*, 1972, **94**, 5082; (*d*) C. E. Barnes and M. R. Dial, *Organometallics*, 1988, **7**, 782; (*e*) C. E. Barnes, J. A. Orvis, D. L. Staley, A. L. Rheingold and D. C. Johnson, *J. Am. Chem. Soc.*, 1989, **111**, 4992.
35 Attempts to model the magnetic susceptibility for compound **3** using various exchange models failed to reproduce the data,† see Fig. S35–37.
36 F. J. Litterst and G. Amthauer, *Phys. Chem. Miner.*, 1984, **10**, 250.
37 (*a*) J. Bertrand, F. A. Cotton and W. A. Dollase, *J. Am. Chem. Soc.*, 1963, **85**, 1349; (*b*) F. A. Cotton and T. E. Haas, *Inorg. Chem.*, 1964, **3**, 10.
38 (*a*) G. Johansson and W. N. Lipscomb, *Acta Crystallogr.*, 1958, **11**, 594; (*b*) A. S. Foust and L. F. Dahl, *J. Am. Chem. Soc.*, 1970, **92**, 7337; (*c*) G. L. Simon and L. F. Dahl, *J. Am. Chem. Soc.*, 1973, **95**, 2164; (*d*) G. L. Simon and L. F. Dahl, *J. Am. Chem. Soc.*, 1973, **95**, 2175; (*e*) C. T.-W. Chu, R. S. Gall and L. F. Dahl, *J. Am. Chem. Soc.*, 1982, **104**, 737; (*f*) G. G. Hoffman, J. K. Bashkin and M. Karplus, *J. Am. Chem. Soc.*, 1990, **112**, 8705; (*g*) A. Agresti, M. Acci, F. Cecconi, C. A. Ghilardi and S. Midollini, *Inorg. Chem.*, 1985, **24**, 689; (*h*) A. Bencini, C. A. Ghilardi, S. Midollini, A. Orlandini, U. Russo, M. G. Uytterhoeven and C. Zanchini, *J. Chem. Soc., Dalton Trans.*, 1995, 963.